

Diffusion Prism: Enhancing Diversity and Morphology Consistency in Mask-to-Image Diffusion

Hao Wang¹, Xiwen Chen¹, Ashish Bastola¹, Jiayou Qin², and Abolfazl Razi^{1*}

¹Clemson University

²Stevens Institute of Technology

{hao9, xiwenc, abastol}@g.clemson.edu, jqin6@stevens.edu, arazi@clemson.edu

Abstract

The emergence of generative AI and controllable diffusion has made image-to-image synthesis increasingly practical and efficient. However, when input images exhibit low entropy and sparsity, the inherent characteristics of diffusion models often result in limited diversity. This constraint significantly interferes with data augmentation in many fields. To address this, we propose **Diffusion Prism**, a training-free framework that efficiently transforms binary masks into realistic and diverse samples while preserving morphological features. We explored that a small amount of artificial noise will significantly assist the image-denoising process. To prove this novel mask-to-image concept, we use nano-dendritic patterns as an example to demonstrate the merit of our method compared to existing controllable diffusion models. Furthermore, we extend the proposed framework to other biological patterns, highlighting its potential applications across various fields. Our source code and sample datasets are available at: <https://arazi2.github.io/aisends.github.io/project/Prism>

1. Introduction

Image quality plays an important role in various data-scarce domains. For instance, research in biometrics, material science, and medical imaging [17, 21] heavily relies on high-quality raw data, precise annotation, and effective data augmentation to overcome the lack of sufficient datasets [13, 23, 29]. With deep learning dominant in recent research, high-quality data pre-processing and efficient utilization lay a solid foundation for downstream tasks such as segmentation, detection, recognition, and classification [1, 12, 37, 38, 45].

Recently, generative models such as GANs (Generative Adversarial Networks), have demonstrated the ability to generate realistic images for data synthesis [19, 37, 46], en-

*Corresponding author

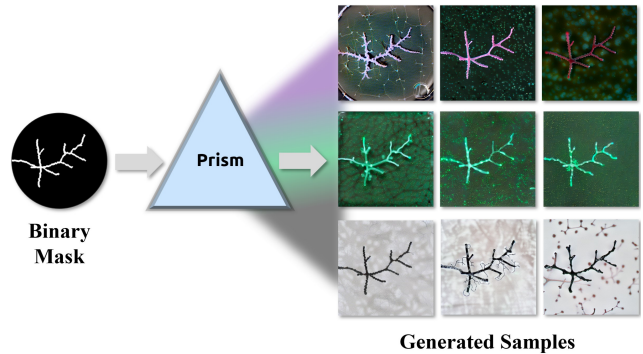


Figure 1. Concept of the Diffusion Prism

abling researchers to expand datasets with minimal manual effort. More approaches such as style transfer, have also been widely used to transform existing images into new ones with specified styles [10, 36]. However, these methods exhibit inherent limitations: their reliance on pre-defined style templates constrains their ability to generate truly novel and diverse samples, and their need for computationally expensive fine-tuning or retraining reduces their practicality [16, 31].

Latent diffusion models have rapidly become the dominant framework for high-quality image generation across various computer vision tasks [26]. Using textual prompts allows the synthesis of semantically rich and visually detailed images [4, 22], with applications spanning digital arts and content creation [20, 43]. Recent research further introduced controllable generation frameworks, such as ControlNet and Uni-ControlNet [40, 42], that enhance the flexibility of diffusion models by incorporating input-specific images (pose map, depth map, etc.) as structural guides. These developments have significantly improved the precision and applicability of AI-generated content, especially in fields such as design and manufacturing [39].

While these frameworks excel in entertainment and creative industries, the gap still exists between their practical application and conventional scientific research such

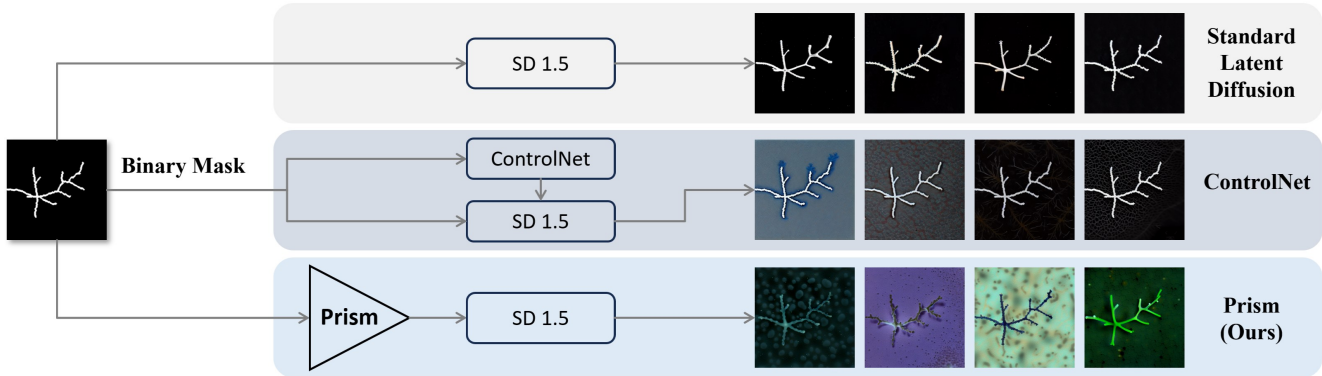


Figure 2. Comparison of different diffusion frameworks. The proposed method Prism is an individual add-on module that does not require any training and does not interact with the vanilla diffusion model

as material science and medical imaging [14, 15, 35]. In these fields, the ability to generate realistic and diverse samples from sparse binary masks could enable transformative advances in data augmentation and morphological analysis [23]. However, we identify a major limitation in existing controllable diffusion methods: lack of image diversity when working with sparse inputs. These challenges arise from the denoising process, where sparse inputs fail to guide the generation of rich and complex outputs.

To address the challenge of generating realistic samples from binary masks, we propose the **Diffusion Prism**, a simple yet efficient method that requires no additional training or fine-tuning of the diffusion model. The Diffusion Prism is an individual add-on module that is based on the pre-trained Stable Diffusion v1.5 (SD1.5) [26] and only modulates the input images in the pixel space to achieve domain shift without altering the diffusion model’s parameters, similar to light refraction through a prism in the real world, as shown in Figure 1. The Diffusion Prism enhances both the diversity and texture of generated images with morphological consistency by introducing controllable noise and chromatic aberration into the input. For convenience, we use the term **Prism** to represent this proposed method in the rest of the paper.

Our contribution can be summarized as:

- **Training-Free Framework:** Our proposed method requires no additional training or fine-tuning.
- **Morphology Consistency:** We employ a lower denoising strength to preserve the morphological information from the input manually.
- **Enhanced Diversity:** By manipulating the input image in the pixel domain, it effectively expands the diversity of input images.

To prove this novel mask-to-image concept, we employ the nano-dendritic patterns – a mathematically generated

high-entropy random patterns – as an example in our experiments to showcase the feature of our method. The results demonstrate that the proposed Prism can significantly improve the image diversity of dendritic samples, while not sacrificing the integrity of morphology structures of the input binary mask.

2. Related Work

2.1. Dendritic Patterns

Dendritic patterns, a class of nano-scale digital tokens, have emerged as highly representative structures for studying and advancing biometric and security applications [8, 34]. These patterns, formed through stochastic natural processes, are characterized by their distinctive morphological features, high entropy, and randomness [5, 28]. Unlike traditional biometric traits, dendritic patterns can encode vast amounts of multidimensional information while remaining resistant to reverse engineering and prediction [2, 3]. Furthermore, their structural complexity can be mathematically modeled, providing researchers with an ideal tool for exploring the intricate characteristics of biological information and developing novel security frameworks [33], as shown in Figure 3.

However, the lack of annotated datasets for these structures presents a major challenge, as capturing their intricate geometry and fine details is both labor-intensive and costly [15]. Thus, a method to generate mask-to-image pairs is valuable for downstream tasks including segmentation, object recognition, and skeleton extraction, as the masks serve as ground truth for the generated images [11, 12, 32, 44].

2.2. Image-to-Image Diffusion

A standard latent diffusion model consists of three key components: the Variational Autoencoder (VAE), which compresses high-dimensional input images into a lower-dimensional latent space to reduce computational complexity; the denoising U-Net, which refines noisy latent rep-

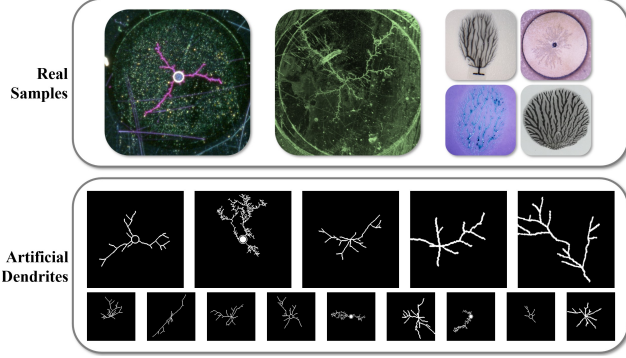


Figure 3. Dendrite samples. Real samples (upper) are taken in lab microscopes; Artificial samples (lower) are generated using mathematical algorithms

representations into coherent outputs; and a CLIP-based tokenizer that bridges the gap between textual prompts and images [25]. Together, these components enable the efficient synthesis of semantically rich and visually detailed images [26].

As the demand for more control over the generation process grew, models such as ControlNet introduced the controllable image-to-image diffusion, allowing precise control over generated content by incorporating structural guides such as masks and sketches [40, 42]. These methods have proven effective in industrial applications, where generated content must meet specific structural and stylistic requirements [39].

Despite their success, existing controllable diffusion frameworks face critical limitations when applied to sparse inputs. As shown in Figure 2, sparse binary masks fail to guide the generation of wealthy and diverse content. This is partially because, in controllable diffusion architecture, the controlling network mostly guides the high-frequency signals from the conditional images, thus preserving the morphology from the input [42]. However, due to a strong relation between the initial image and the final decoded tensor, a sparse input can hardly generate high-entropy information by only relying on the denoising sampler [7].

3. Methodology

The sparse and low-entropy nature of binary masks makes the denoising process difficult, as the randomness introduced during diffusion is often insufficient to generate diverse backgrounds. To address this, we proposed our method based on a pre-trained Stable Diffusion v1.5 to explore the image denoising process.

3.1. Signal Degradation in Denoising

The uncertainty introduced by high-denoising strength is a key challenge in image-to-image translation. Al-

though high denoising strength increases diversity, it degrades high-frequency information, removing important information that may contain morphological details. This causes parts of the input image in the latent space to be treated as noise, making it difficult to maintain morphological consistency with the input, as illustrated in Figure 5.

To examine the details, we formulate the problem by using the vanilla DDIM sampler from latent diffusion [26, 27]. The initial latent tensor z is generated during forward diffusion using the following equation:

$$z_t = \alpha_t \cdot x_0 + \sqrt{1 - \alpha_t} \cdot \epsilon. \quad (1)$$

Here, α_t controls how much of the original image x_0 is retained over time t , while ϵ , sampled from a Gaussian distribution $\epsilon \sim \mathcal{N}(0, 1)$, represents the latent noise added to obscure the image. In the denoising (reverse diffusion) process, as t increases, the denoise sampler will predict a higher amount of noise at the initial step, as shown in Figure 5(a)(b). As a consequence, the influence of the input image diminishes, and noise becomes more dominant, leading to signal degradation and loss of high-frequency details, as shown in Figure 5. This explains the phenomenon that increasing the denoising strength introduces more randomness but also increases the risk of losing critical information from the input image. To balance morphology consistency and diversity, a lower denoising strength is often recommended.

3.2. Initial Entropy

When using lower strength during denoising, we found that binary input images, such as masks, fail to produce diverse outputs. Such low-entropy images often produce minimal visual content because they lack sufficient randomness. This also explains why mainstream text-to-image models start with random matrices to provide the necessary diversity for effective image generation [26].

We found that introducing artificial signals into the initial image can significantly influence the denoising process. These artificial signals will be misinterpreted as noise, which affects the prediction of noise and the calculation of the noiseless tensor z_0 . Specifically, the process can be expressed as:

$$z'_t = \mathcal{E}(x + n) \quad (2)$$

$$\epsilon_\theta(z'_t, t) = \epsilon_\theta(z_t, t) + \delta \quad (3)$$

Here, \mathcal{E} is the encoder of the pre-trained VAE, n represents the introduced signal, ϵ_θ is the predicted noise at step t , and δ is the residual term at step t that is introduced by the signal n during encoding. As the predicted noise changes, the noiseless tensor z_0 also alters:

$$z'_0 = \frac{z_t - \sqrt{1 - \alpha_t}(\epsilon_\theta(z_t, t) + \delta)}{\sqrt{\alpha_t}}, \quad (4)$$

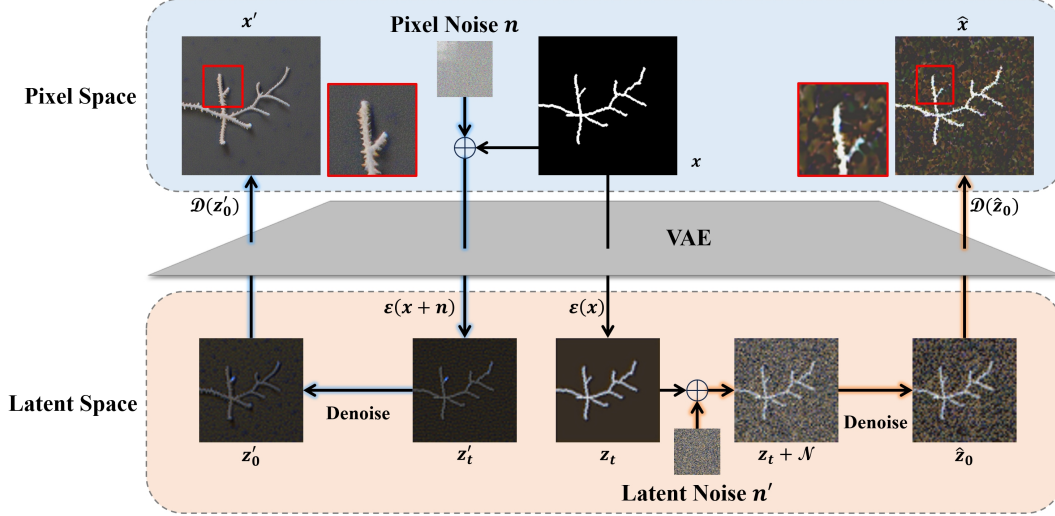


Figure 4. Noise injection comparison: pixel space vs. latent space.

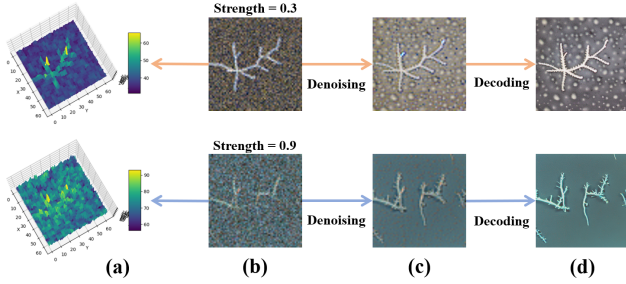


Figure 5. Noise sampling schedule in image-to-image synthesis.

$$\begin{aligned} z'_0 &= z_0 - \frac{\sqrt{1 - \alpha_t}}{\sqrt{\alpha_t}} \delta \\ &= z_0 - \hat{\alpha} \delta. \end{aligned} \quad (5)$$

Here, the term $\hat{\alpha} \delta$ represents the introduced information in the latent space. By adding n to the initial image, the additional signal becomes part of the image content rather than being treated as noise due to the domain shift, as shown in Figure 4. This ensures the consistency of the denoising steps while enriching the content, resulting in more detailed final images.

3.3. Domain Shift in Diffusion

There exist two possible ways to achieve domain shift in diffusion: pixel-level operations and latent space operations [7]. However, due to the different characteristics of the image in the pixel domain versus the latent space, manipulating in latent space is risky. For instance, the latent diffusion process can be simplified as:

$$\hat{x} = \mathcal{D}(z) = \mathcal{D}(\mathcal{E}(x)), \quad (6)$$

where x is the input image, \mathcal{E} and \mathcal{D} are the encoder and decoder of the pre-trained VAE, z is the latent tensor, and \hat{x}

is the denoised image [26].

Thus, making any changes directly in the latent space tends to result in corrupted images in the pixel domain. As shown in Figure 4, altering the content of the latent tensor may shatter the representation of the image in latent space. Additionally, to align the latent tensor with the intended transformation, retraining or fine-tuning the model is often required [6]. In contrast, the translation from pixel to latent space effectively projects the pixel distribution into the latent distribution. This process ensures that all information present in the pixel space is coupled into the latent space, making it easier to fuse with text features.

3.4. Diffusion Prism

As proved in Section 3.3, latent operation poses a high risk of domain collapse. Thus, in this paper, we employ image manipulation in the pixel domain, which allows for minimal yet effective transformations by introducing artificial signals or noise. In addition to blending noise into the initial image, we also introduce *chromatic aberration* as an additional form of domain warping. This process involves shuffling pixel values across channels, which simulates optical distortion without compromising the structural integrity of the input image.

When using Prism in practical applications, we typically derive the mean and standard deviation from a reference image to emulate a specific style, as shown in Figure 1. However, in the experiments, we use a random matrix as the sample image I to ensure maximum diversity. Specifically, we evaluate the pixel distribution in each color channel by calculating:

$$\mu = \frac{1}{N} \sum_{x,y} I(x,y), \quad (7)$$

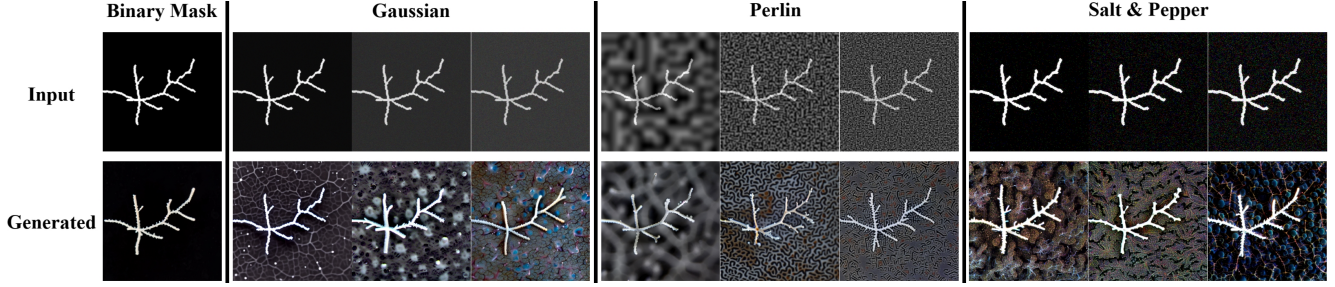


Figure 6. Noise type comparison, the input are binary mask with different types of noise, and the outputs are the generated images with the proposed method.

$$\sigma = \sqrt{\frac{1}{N} \sum_{x,y} (I(x,y) - \mu)^2}, \quad (8)$$

where μ and σ are the mean and standard deviation of the pixel values, N is the total number of pixels in a sample image I , and $I(x,y)$ is the pixel value at position (x,y) . Furthermore, we incorporate the original color information with μ and σ into the mask M , along with artificial noise n :

$$n \sim \mathcal{N}(\mu, \sigma) \quad (9)$$

$$M(x,y) = (M(x,y) \cdot \sigma + \mu) + n \quad (10)$$

This process introduces controlled variations via samples from a standard normal distribution. Note that this normal distribution is different than the denoise sampler, as mentioned in Equation 1. This approach ensures that the generated image has both structural integrity from the mask and sufficient visual variability from the added artificial noise.

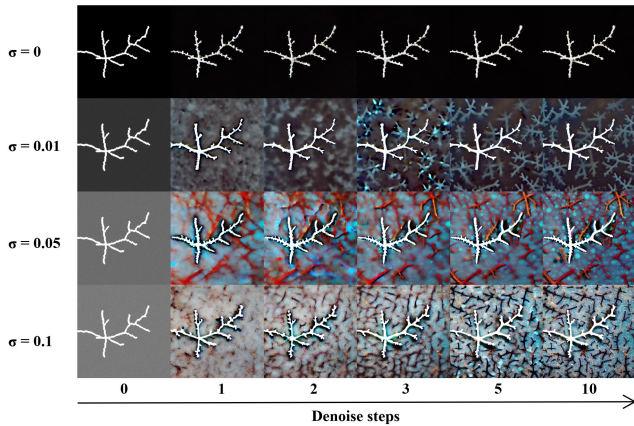


Figure 7. Mask diffusion process: adding Gaussian noise into the input image can increase the richness of the background. Denoising step: 10, text prompt scale: 10, denoising strength: 0.3, text prompt: "a dendrite sample".

3.5. Impact of Noise in Prism

To further explore how adding artificial noise to the initial image affects the diversity of the generated image and

background details, Gaussian noise with varying standard deviation σ was introduced at the pixel level, as shown in Figure 7. As a result, Figure 7 demonstrates the significant impact that noise has on the diversity of the generated images. When noise is introduced into the initial images, even in small amounts, it drastically alters the background texture, resulting in richer and more varied background details compared to images generated from noise-free inputs. This is also validated in the Table 1. The degree of diversity in the final images is directly proportional to the amount of noise added to the initial image, supporting our hypothesis outlined in Section 3.

In addition, we investigated how different types of noise affect the richness and detail of the generated images. We experimented with various types of noise, including Gaussian noise, salt-and-pepper noise, and Perlin noise [9], by applying each to the initial image and measuring the resulting information entropy. As shown in Figure 6, even a small amount of artificial signal can enhance background synthesis, and different types of noise lead to varying levels of background detail in the generated images. For instance, coarse noise patterns tend to generate blurred backgrounds, while fine noise results in more intricate textures, as shown in Figure 6.

4. Experiments

Our experiments focus on evaluating two key aspects of the generated dendrite samples: data diversity and morphology consistency to the input masks. Then, we compare our proposed method (Prism) against other approaches using conventional evaluation metrics.

4.1. Qualitative Results

Figure 8 presents the qualitative results generated by different diffusion frameworks, including standard latent diffusion [26], control-based diffusion methods [40, 42], and the proposed Diffusion Prism. The inputs are binary masks, and the outputs are image-to-image diffusion-generated samples. As shown in the figure, vanilla SD1.5 produces realistic samples; however, as the denoising strength increases,

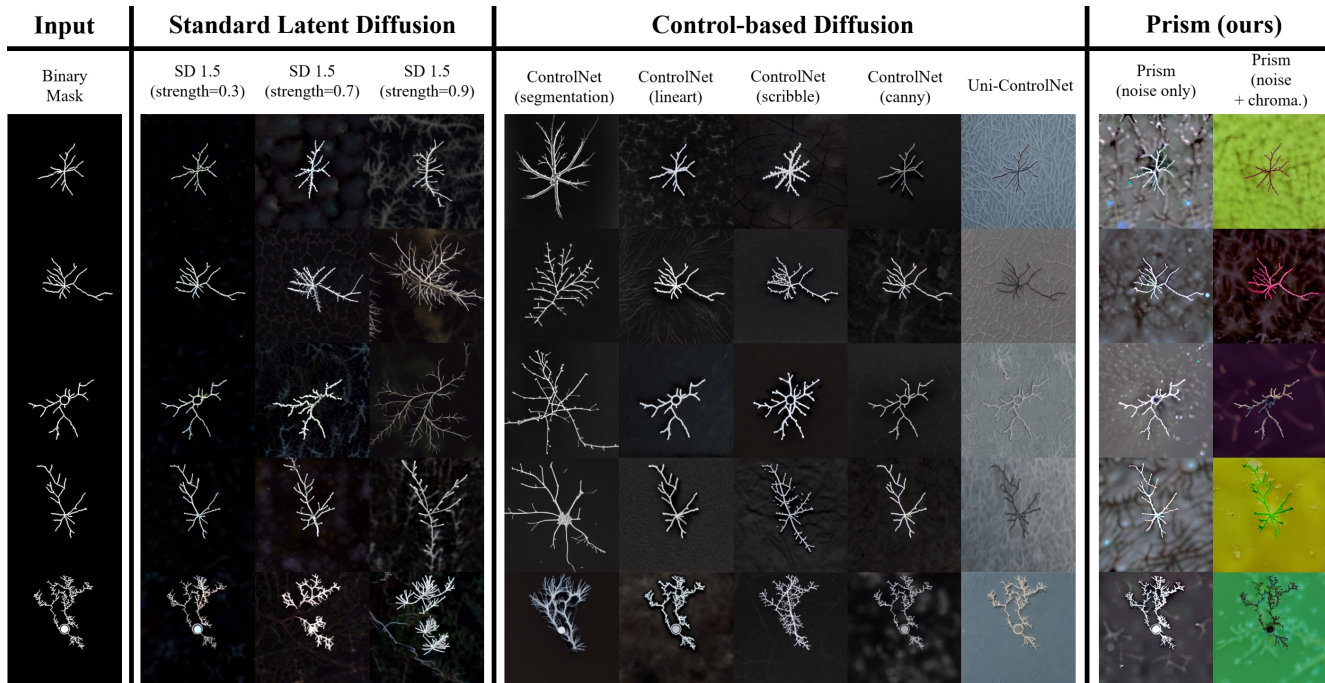


Figure 8. Qualitative test. We use three different diffusion frameworks (standard latent diffusion, control-based diffusion, and our method) to obtain sample datasets. The input is a binary mask and all frameworks use image-to-image diffusion to generate samples.

significant morphological details are lost. ControlNet, when paired with a specific preprocessor (Canny), achieves better results than other preprocessors, yet the generated backgrounds still lack diversity. Uni-ControlNet improves both diversity and morphological consistency, addressing some of these issues. In comparison, the proposed Diffusion Prism demonstrates superior performance in both visual realism and diversity, achieving the best overall quality among the evaluated methods.

4.2. Quantitative evaluation

To quantitatively assess the performance of our method, we conduct comparisons with both vanilla SD1.5 (Stable Diffusion v1.5) [26], ControlNet (SD1.5) [40], and Uni-ControlNet (SD 1.5) [42]. For fairness, we applied the Prism module to the vanilla SD1.5 and kept the diffusion parameters consistent across all experiments. Specifically,

- Denoising steps, refer to the number of iterations in the denoising process, we use 10 in all experiments.
- Denoising strength, controls the balance between noise and the input image during the generation process. We use the value 0.3 in the vanilla SD 1.5 and the proposed Prism experiments to ensure the morphology consistency as explained in Section 3, and we use the value 0.99 in other control-based diffusion methods to ensure maximum variation since their morphology will be less impacted by the denoising strength.

- Text prompt: The text prompt used in all cases is set to *"a realistic dendrite sample"* to ensure consistency across different models.
- The text prompt scale controls how strongly the model adheres to the text prompt during image generation, also known as the guidance scale. We use 10 in all experiments.

In the proposed Prism method, we apply standard Gaussian noise with a mean of $\mu = 0$ and set the color sampling to complete randomness ($I \sim \mathcal{N}$). To analyze the impact on morphology and diversity, we varied the standard deviation σ of the noise from 0 to 1.

Normalized FID (nFID): The **Fréchet Inception Distance (FID)** is a widely used metric for evaluating the quality and diversity of generated images by comparing their distribution to real images [30,36]. In our experiments, we compute the Normalized FID (nFID) by comparing the images generated using Prism and other diffusion approaches against those from a baseline model (SD 1.5). A lower nFID value indicates that the generated images are more structurally and texturally similar to the ground truth. We utilize the EMDS-6 dataset [41], which closely matches the style of the real dendritic patterns, to calculate the nFID [6]. The features for this calculation are extracted using the standard Inception model [30] provided in the `torchvision` package from `PyTorch`. For the evaluation, we prepared multiple noise settings, generating 10,000 images for each

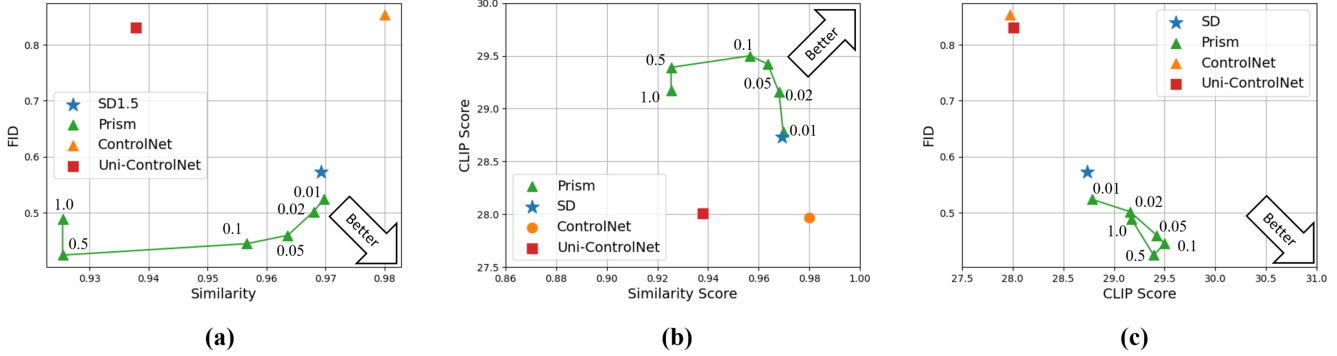


Figure 9. Model performance comparison. (a) is the nFID-SSIM plot, (b) is the CLIP-SSIM plot, and (c) is the nFID-CLIP plot

setting to compute and normalize the FID scores.

Morphology Similarity: To assess morphology consistency, we extract the binary masks from the generated samples using random forest and then compute the structural similarity index measure (SSIM) between the binary mask and the generated image [24]. This method is reliable and accurate as the original binary masks can be used for ground-truth labels to supervise the random forest model. The SSIM algorithm captures structural similarities and enables the evaluation of how well the generated images preserve the structure of the input. The detailed experiment process is shown in Figure 10. For convenience, we use the ControlNet with the canny method for comparison due to its better performance, as shown in Figure 8.

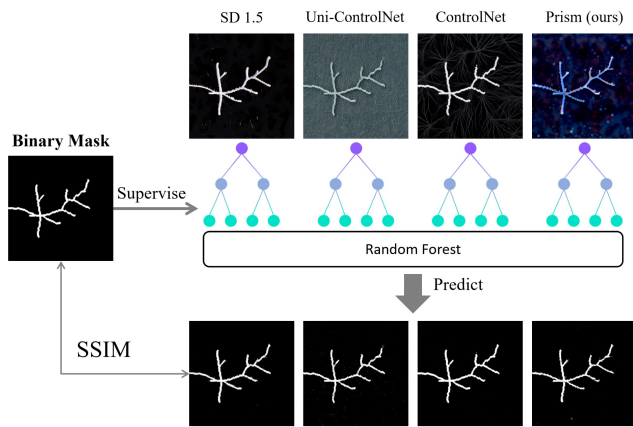


Figure 10. Process of SSIM calculation. Supervised random forest models will be used to predict the mask of generated samples, then the SSIM will be calculated based on the predictions and ground truth

CLIP Score: Additionally, we measure the text-image similarity through the CLIP Score, which measures how well the generated images align with the textual or visual prompts [25]. We use the same CLIP (ViT-B/32) model, which encodes both images and texts into a shared embedding space. A higher CLIP Score indicates that the generated images better align with the semantics of the input

prompt.

Table 1. Performance Comparison

Method	nFID-10k ↓	CLIP Score ↑	SSIM ↑
SD1.5 [26]	0.6039	28.73	0.9692
ControlNet (Best) [40]	0.8531	27.97	0.9801
Uni-ControlNet [42]	0.8311	28.01	0.9378
Fully Random (denoise strength = 1.0)	0.8893	27.77	0.5067
Prism (noise Std. = 0.01)	0.5238	28.78	0.9697
Prism (noise Std. = 0.05)	0.4594	29.42	0.9636
Prism (noise Std. = 0.1)	0.4444	29.47	0.9566
Prism (noise Std. = 0.5)	0.4241	29.40	0.9254
Prism (noise Std. = 1.0)	0.4887	29.19	0.9254

FID-Similarity Test: For reference, we use full denoising strength (1.0) to represent the fully random samples, as shown in Table 1. As illustrated in Figure 9(a), ControlNet achieves the highest CLIP similarity score, indicating that the morphology of its generated images is closely aligned with the input masks. However, its FID score remains high, indicating lower quality. As illustrated in Figure 8, although the input image’s structure is well preserved, it does not blend seamlessly with the generated background.

In contrast, the images generated by Prism, with a noise level of $\sigma = 0.01$, maintain a comparable SSIM (0.92 – 0.97) while enhancing diversity, as shown in Table 1. As the noise level increases, the FID continues to improve until $\sigma = 0.5$. Beyond this point, excessive noise degrades the input signal in the pixel space, leading to a reduction in both image quality and similarity.

CLIP Score-Similarity Test: As shown in Figure 9(b), Prism-generated images achieve higher CLIP scores due to their diverse backgrounds and realistic dendritic patterns. In comparison, the CLIP score of ControlNet falls below that of vanilla SD 1.5, suggesting that controllable image-to-image diffusion models such as ControlNet and Uni-ControlNet may not be optimal for this particular task.

FID-CLIP Score Test: As demonstrated in Figure 9(c), Prism consistently outperforms other methods in both text-image alignment and diversity without significantly compromising image similarity. This balance showcases

Prism’s ability to generate visually diverse and semantically consistent images.

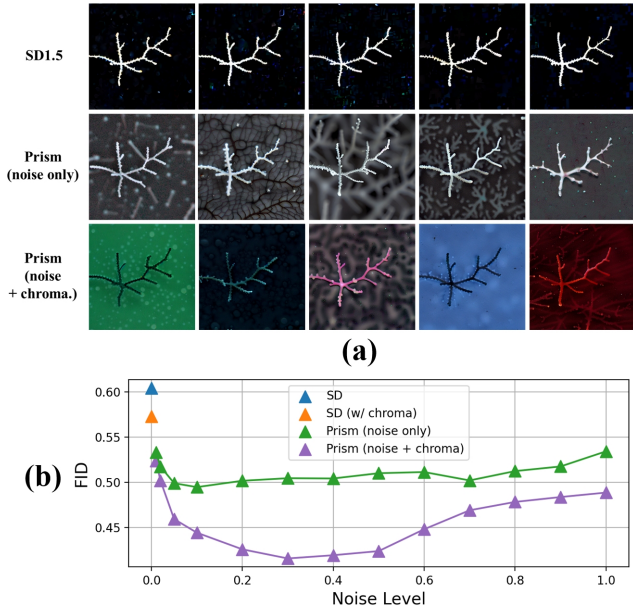


Figure 11. Ablation study. (a) demonstrate the visual effect of the proposed noise module and chromatic aberration. (b) shows the effect of different modules in terms of nFID score.

4.3. Ablation Study

In this section, we evaluate the two key components of the Prism: controllable noise and chromatic aberration. As shown in Figure 11(b), we conducted tests to measure the FID of generated images under different settings. The results demonstrate that both noise injection and chromatic aberration significantly enhance image quality and diversity. Notably, the inclusion of chromatic aberration allows for a more effective use of noise, leading to better results compared to the noise-only approach, as shown in Figure 11(a). Table 2 shows that not only the quality of the image can be improved with both modules, but also they boost the text-image alignment and the morphology consistency. The combination of these two techniques results in more diverse and higher-quality outputs, confirming their importance in improving the overall performance of the model.

Table 2. Ablation Study

Method (best)	nFID-10k ↓	CLIP Score ↑	SSIM ↑
SD1.5	0.6039	28.73	0.9692
SD+Prism (noise-only)	0.5330 (-0.0709)	28.78 (-0.05)	0.9718 (-0.0026)
SD+Prism (chroma-only)	0.5727 (-0.0312)	29.03 (-0.30)	0.9726 (-0.0034)
SD+Prism (noise+chroma)	0.4241 (-0.1798)	29.47 (-0.74)	0.9697 (-0.0005)

5. Discussion

We further evaluated the potential of the proposed Diffusion Prism for data augmentation across other biometric ap-

plications. Specifically, Figure 12 illustrates its application to enhancing binary masks of the retina fundus pattern [29], the fingerprint sample [33], and the Purkinje neuron sample [18]. The generated samples present realistic styles and diverse backgrounds while maintaining consistent morphology aligned with the input binary masks, which proved the adaptability and effectiveness in other domains.

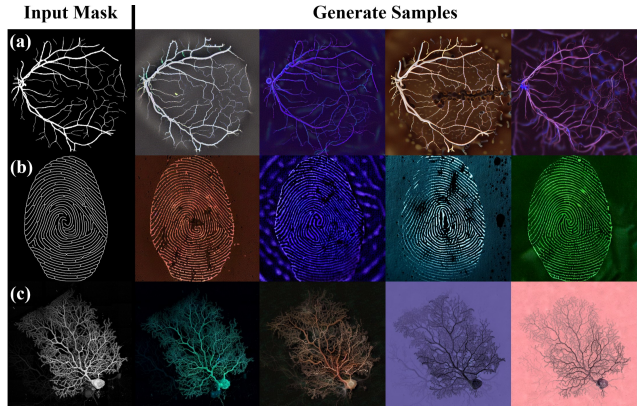


Figure 12. Diffusion Prism in biometric applications. (a) is Retina Fundus mask with text prompt: "a realistic retina fundus sample", (b) is Fingerprint mask with text prompt: "a broken fingerprint with ink", and (c) is Purkinje neuron mask, with text prompt: "a realistic neuron sample"

6. Conclusion

In this paper, we presented the Diffusion Prism, a simple yet effective technique for generating diverse and morphologically consistent images from sparse binary masks. After comprehensively analyzing the signal transmission in image-to-image diffusion, we proposed an effective combination of controlled noise and chromatic aberration to enhance diversity without sacrificing the structural integrity of the input masks. The experimental results on dendritic patterns demonstrated that our method significantly improves the diversity of generated images, outperforming baseline and other methods in both quantitative evaluations and visual comparisons. We also performed the method on other biometric samples, which offers a promising mask-to-image solution in various practical applications.

Acknowledgments

This material is based upon the work supported by the National Science Foundation under Grant Number 2204721 and partially supported by our collaborative project with MIT Lincoln Lab under Grant Number 7000612889.

The authors would like to thank Dr. Siyu Huang for his comments on experiment designs.

References

- [1] Lorenza Bonaldi, Andrea Pretto, Carmelo Pirri, Francesca Uccheddu, Chiara Giulia Fontanella, and Carla Stecco. Deep learning-based medical images segmentation of musculoskeletal anatomical structures: a survey of bottlenecks and strategies. *Bioengineering*, 10(2):137, 2023. [1](#)
- [2] Xiwen Chen, Hao Wang, Abolfazl Razi, Michael Kozicki, and Christopher Mann. Dh-gan: a physics-driven untrained generative adversarial network for holographic imaging. *Optics Express*, 31(6):10114–10135, 2023. [2](#)
- [3] Xiwen Chen, Hao Wang, Zhao Zhang, Zhenmin Li, Huayu Li, Tong Ye, and Abolfazl Razi. Enhancing digital hologram reconstruction using reverse-attention loss for untrained physics-driven deep learning models with uncertain distance. In *AI and Optical Data Sciences V*, volume 12903, pages 132–141. SPIE, 2024. [2](#)
- [4] Jooyoung Choi, Yunjey Choi, Yunji Kim, Junho Kim, and Sungroh Yoon. Custom-edit: Text-guided image editing with customized diffusion models. *arXiv preprint arXiv:2305.15779*, 2023. [1](#)
- [5] Hermann Cuntz, Alexander Borst, and Idan Segev. Optimization principles of dendritic structure. *Theoretical Biology and Medical Modelling*, 4:1–8, 2007. [2](#)
- [6] Martin Nicolas Everaert, Marco Bocchio, Sami Arpa, Sabine Süssstrunk, and Radhakrishna Achanta. Diffusion in style. In *Proceedings of the IEEE/CVF International Conference on Computer Vision*, pages 2251–2261, 2023. [4](#), [6](#)
- [7] Martin Nicolas Everaert, Athanasios Fitsios, Marco Bocchio, Sami Arpa, Sabine Süssstrunk, and Radhakrishna Achanta. Exploiting the signal-leak bias in diffusion models. In *Proceedings of the IEEE/CVF Winter Conference on Applications of Computer Vision*, pages 4025–4034, 2024. [3](#), [4](#)
- [8] Meiling Fang, Wufei Yang, Arjan Kuijper, Vitomir Struc, and Naser Damer. Fairness in face presentation attack detection. *Pattern Recognition*, 147:110002, 2024. [2](#)
- [9] Simon Green. Implementing improved perlin noise. *GPU Gems*, 2:409–416, 2005. [5](#)
- [10] Daniel Holden, Ikhsanul Habibie, Ikuo Kusajima, and Taku Komura. Fast neural style transfer for motion data. *IEEE computer graphics and applications*, 37(4):42–49, 2017. [1](#)
- [11] Yasufumi Kawano and Yoshimitsu Aoki. Maskdiffusion: Exploiting pre-trained diffusion models for semantic segmentation. *arXiv preprint arXiv:2403.11194*, 2024. [2](#)
- [12] Alexander Kirillov, Eric Mintun, Nikhila Ravi, Hanzi Mao, Chloe Rolland, Laura Gustafson, Tete Xiao, Spencer Whitehead, Alexander C Berg, Wan-Yen Lo, et al. Segment anything. *arXiv preprint arXiv:2304.02643*, 2023. [1](#), [2](#)
- [13] Avisek Lahiri, Vineet Jain, Arnab Mondal, and Prabir Kumar Biswas. Retinal vessel segmentation under extreme low annotation: A gan based semi-supervised approach. In *2020 IEEE international conference on image processing (ICIP)*, pages 418–422. IEEE, 2020. [1](#)
- [14] Kang-Hyun Lee and Gun Jin Yun. Microstructure reconstruction using diffusion-based generative models. *Mechanics of Advanced Materials and Structures*, 31(18):4443–4461, 2024. [2](#)
- [15] Ruoqian Lin, Rui Zhang, Chunyang Wang, Xiao-Qing Yang, and Huolin L Xin. Temimagenet training library and atom-segnet deep-learning models for high-precision atom segmentation, localization, denoising, and deblurring of atomic-resolution images. *Scientific reports*, 11(1):5386, 2021. [2](#)
- [16] Mohamed Loey, Gunasekaran Manogaran, and Nour Eldeen M Khalifa. A deep transfer learning model with classical data augmentation and cgan to detect covid-19 from chest ct radiography digital images. *Neural Computing and Applications*, pages 1–13, 2020. [1](#)
- [17] Jun Ma, Yuting He, Feifei Li, Lin Han, Chenyu You, and Bo Wang. Segment anything in medical images. *Nature Communications*, 15(1):654, 2024. [1](#)
- [18] Martone Maryann, Price Diana, Thor Andrea, Terada Masako, and Hakozi Hiro. mus musculus, purkinje neuron. cil. dataset., 2002. CCDB:3687. [8](#)
- [19] Andrew Melnik, Maksim Miasayedzenkau, Dzianis Makaravets, Dzianis Pirshtuk, Eren Akbulut, Dennis Holzmann, Tarek Renusch, Gustav Reichert, and Helge Ritter. Face generation and editing with stylegan: A survey. *IEEE Transactions on Pattern Analysis and Machine Intelligence*, 2024. [1](#)
- [20] Chenlin Meng, Yutong He, Yang Song, Jiaming Song, Jiajun Wu, Jun-Yan Zhu, and Stefano Ermon. Sdedit: Guided image synthesis and editing with stochastic differential equations. *arXiv preprint arXiv:2108.01073*, 2021. [1](#)
- [21] Shervin Minaee, Amirali Abdolrashidi, Hang Su, Mohammed Bennamoun, and David Zhang. Biometrics recognition using deep learning: A survey. *Artificial Intelligence Review*, 56(8):8647–8695, 2023. [1](#)
- [22] Ron Mokady, Amir Hertz, Kfir Aberman, Yael Pritch, and Daniel Cohen-Or. Null-text inversion for editing real images using guided diffusion models. In *Proceedings of the IEEE/CVF Conference on Computer Vision and Pattern Recognition*, pages 6038–6047, 2023. [1](#)
- [23] Muzaffer Özbey, Onat Dalmaç, Salman UH Dar, Hasan A Bedel, Şaban Öztürk, Alper Güngör, and Tolga Çukur. Un-supervised medical image translation with adversarial diffusion models. *IEEE Transactions on Medical Imaging*, 2023. [1](#), [2](#)
- [24] Walter HL Pinaya, Petru-Daniel Tudosi, Jessica Dafflon, Pedro F Da Costa, Virginia Fernandez, Parashkev Nachev, Sebastien Ourselin, and M Jorge Cardoso. Brain imaging generation with latent diffusion models. In *MICCAI Workshop on Deep Generative Models*, pages 117–126. Springer, 2022. [7](#)
- [25] Alec Radford, Jong Wook Kim, Chris Hallacy, Aditya Ramesh, Gabriel Goh, Sandhini Agarwal, Girish Sastry, Amanda Askell, Pamela Mishkin, Jack Clark, et al. Learning transferable visual models from natural language supervision. In *International conference on machine learning*, pages 8748–8763. PMLR, 2021. [3](#), [7](#)
- [26] Robin Rombach, Andreas Blattmann, Dominik Lorenz, Patrick Esser, and Björn Ommer. High-resolution image synthesis with latent diffusion models. In *Proceedings of the IEEE/CVF conference on computer vision and pattern recognition*, pages 10684–10695, 2022. [1](#), [2](#), [3](#), [4](#), [5](#), [6](#), [7](#)

- [27] Jiaming Song, Chenlin Meng, and Stefano Ermon. Denoising diffusion implicit models. *arXiv preprint arXiv:2010.02502*, 2020. [3](#)
- [28] Nelson Spruston. Pyramidal neurons: dendritic structure and synaptic integration. *Nature Reviews Neuroscience*, 9(3):206–221, 2008. [2](#)
- [29] J. Staal, M.D. Abramoff, M. Niemeijer, M.A. Viergever, and B. van Ginneken. Ridge-based vessel segmentation in color images of the retina. *IEEE Transactions on Medical Imaging*, 23(4):501–509, 2004. [1](#), [8](#)
- [30] Christian Szegedy, Vincent Vanhoucke, Sergey Ioffe, Jon Shlens, and Zbigniew Wojna. Rethinking the inception architecture for computer vision. In *Proceedings of the IEEE conference on computer vision and pattern recognition*, pages 2818–2826, 2016. [6](#)
- [31] Reihaneh Torkzadehmahani, Peter Kairouz, and Benedict Paten. Dp-cgan: Differentially private synthetic data and label generation. In *Proceedings of the IEEE/CVF Conference on Computer Vision and Pattern Recognition Workshops*, pages 0–0, 2019. [1](#)
- [32] Hao Wang, Sayed Pedram Haeri Boroujeni, Xiwen Chen, Ashish Bastola, Huayu Li, Wenhui Zhu, and Abolfazl Razi. Flame diffuser: Wildfire image synthesis using mask guided diffusion. *arXiv preprint arXiv:2403.03463*, 2024. [2](#)
- [33] Hao Wang, Xiwen Chen, Abolfazl Razi, and Rahul Amin. Fast Key Points Detection and Matching for Tree-Structured Images. In *2022 International Conference on Computational Science and Computational Intelligence (CSCI)*, pages 1381–1387, Los Alamitos, CA, USA, Dec. 2022. IEEE Computer Society. [2](#), [8](#)
- [34] Hao Wang, Xiwen Chen, Abolfazl Razi, Michael Kozicki, Rahul Amin, and Mark Manfredo. Nano-resolution visual identifiers enable secure monitoring in next-generation cyber-physical systems. In *2022 International Conference on Computational Science and Computational Intelligence (CSCI)*, pages 856–861, 2022. [2](#)
- [35] Hao Wang, Wenhui Zhu, Jiayou Qin, Xin Li, Oana Dumitrascu, Xiwen Chen, Peijie Qiu, and Abolfazl Razi. Rbad: A dataset and benchmark for retinal vessels branching angle detection. *arXiv preprint arXiv:2407.12271*, 2024. [2](#)
- [36] Matthias Wright and Björn Ommer. Artfid: Quantitative evaluation of neural style transfer. In *DAGM German Conference on Pattern Recognition*, pages 560–576. Springer, 2022. [1](#), [6](#)
- [37] Cong Wu, Yixuan Zou, and Zhi Yang. U-gan: Generative adversarial networks with u-net for retinal vessel segmentation. In *2019 14th international conference on computer science & education (ICCSE)*, pages 642–646. IEEE, 2019. [1](#)
- [38] Junde Wu, Wei Ji, Huazhu Fu, Min Xu, Yueming Jin, and Yanwu Xu. Medsegdiff-v2: Diffusion-based medical image segmentation with transformer. In *Proceedings of the AAAI Conference on Artificial Intelligence*, volume 38, pages 6030–6038, 2024. [1](#)
- [39] Lvmin Zhang and Maneesh Agrawala. Transparent image layer diffusion using latent transparency. *arXiv preprint arXiv:2402.17113*, 2024. [1](#), [3](#)
- [40] Lvmin Zhang, Anyi Rao, and Maneesh Agrawala. Adding conditional control to text-to-image diffusion models. In *Proceedings of the IEEE/CVF International Conference on Computer Vision*, pages 3836–3847, 2023. [1](#), [3](#), [5](#), [6](#), [7](#)
- [41] Peng Zhao, Chen Li, Md Mamunur Rahaman, Hao Xu, Pingli Ma, Hechen Yang, Hongzan Sun, Tao Jiang, Ning Xu, and Marcin Grzegorzec. Emms-6: Environmental microorganism image dataset sixth version for image denoising, segmentation, feature extraction, classification, and detection method evaluation. *Frontiers in Microbiology*, 13:829027, 2022. [6](#)
- [42] Shihao Zhao, Dongdong Chen, Yen-Chun Chen, Jianmin Bao, Shaozhe Hao, Lu Yuan, and Kwan-Yee K Wong. Uni-controlnet: All-in-one control to text-to-image diffusion models. *Advances in Neural Information Processing Systems*, 36, 2024. [1](#), [3](#), [5](#), [6](#), [7](#)
- [43] Linqi Zhou, Aaron Lou, Samar Khanna, and Stefano Ermon. Denoising diffusion bridge models. *arXiv preprint arXiv:2309.16948*, 2023. [1](#)
- [44] Yupeng Zhou, Daquan Zhou, Zuo-Liang Zhu, Yaxing Wang, Qibin Hou, and Jiashi Feng. Maskdiffusion: Boosting text-to-image consistency with conditional mask. *arXiv preprint arXiv:2309.04399*, 2023. [2](#)
- [45] Wenhui Zhu, Peijie Qiu, Xiwen Chen, Huayu Li, Hao Wang, Natasha Lepore, Oana M Dumitrascu, and Yalin Wang. Beyond mobilenet: An improved mobilenet for retinal diseases. In *International Conference on Medical Image Computing and Computer-Assisted Intervention*, pages 56–65. Springer, 2023. [1](#)
- [46] Wenhui Zhu, Peijie Qiu, Oana M Dumitrascu, Jacob M Sobczak, Mohammad Farazi, Zhangsihao Yang, Keshav Nandakumar, and Yalin Wang. Otre: where optimal transport guided unpaired image-to-image translation meets regularization by enhancing. In *International Conference on Information Processing in Medical Imaging*, pages 415–427. Springer, 2023. [1](#)